# Chapter 11
# Two-Dimensional J-Resolved Spectroscopy


## Gareth A. Morris

*Department of Chemistry, University of Manchester, Oxford Road, Manchester, M13 9PL, UK*




### 11.1 INTRODUCTION

J-resolved 2D spectroscopy (also commonly known as 2D J-spectroscopy) is a class of two-dimensional NMR methods which separate chemical shifts from multiplet structure. In pulse sequences for J-resolved 2D spectroscopy, a 180° pulse is applied at the center of the evolution period $t_1$, generating a spin echo. The modulation of spin echoes by scalar coupling causes signals to be dispersed in the $F_1$ domain of the resultant 2D spectrum according to their position within scalar coupling multiplets. This allows the separation of multiplet structure from chemical shifts, improving the resolution of individual signals in spectra with overlapping multiplets. There is a further gain in resolution in the $F_1$ domain of the 2D spectrum because the spin echo suppresses the effects of $B_0$ inhomogeneity, giving $F_1$ linewidths approaching the natural limit $1/(\pi T_2)$. J-resolved 2D spectroscopy is now much less widely used than correlated 2D methods, but still finds application, for example in the analysis of complex spin systems and in the separation of homonuclear from heteronuclear coupling structure.

Both homonuclear and heteronuclear multiplet structure can be investigated by J-resolved spectroscopy. Because the broadband suppression of homonuclear couplings during measurement of the free induction decay is not possible, homonuclear J-resolved 2D spectroscopy[1] produces spectra with multiplet structure in $F_1$, and both multiplet structure and chemical shifts in $F_2$. On the other hand, in heteronuclear J-resolved 2D spectroscopy,[2,3] it is normal to apply broadband decoupling during data acquisition, so that multiplet structure is suppressed in $F_2$ and a complete separation is achieved between multiplet structure in $F_1$ and chemical shifts in $F_2$. For weakly coupled spin systems, a similar separation can be achieved in homonuclear J-resolved 2D spectroscopy by "shearing" or "tilting" the 2D data matrix[1] to give a 45° tilt in frequency space:

$$S(F_1, F_2') = S(F_1, F_2 - F_1) \qquad (11.1)$$

where $F_2' = F_2 - F_1$, so that signals are shifted along the $F_2$ axis by a distance equal to $-F_1$. A further difference between homonuclear and heteronuclear methods lies in the origin of the echo modulation. In the homonuclear experiment, the modulation naturally arises from the action of the 180° pulse that is used to generate the spin echo, because it affects both the partners in any scalar coupling. In the heteronuclear experiment, couplings to heteronuclei that are weakly coupled among themselves do not give rise

to any modulation of the spin echo unless a suitable perturbation is applied to the heteronuclei.

The simplest form of J-resolved spectroscopy is the homonuclear experiment of sequence 11.2, in which the basic Carr–Purcell method A spin echo sequence[4] forms the evolution period of a 2D experiment:

$$90^\circ - t_1/2 - 180^\circ - t_1/2 - \text{Acquire} \qquad (11.2)$$

This experiment is normally used in proton NMR, but is applicable to any nuclei with homonuclear couplings. Because the resulting signals are phase modulated with respect to $t_1$, it is not normally practicable to use phase sensitive display (but see 11.5.2). To secure acceptable absolute value mode lineshapes, it is usual to apply either pseudoecho[5] or sine-bell[6] weighting in both frequency dimensions, despite the signal-to-noise ratio penalty. This forces the time-domain signals into an approximately symmetric envelope, so that dispersion-mode contributions (which have odd symmetry) are absent from the resultant frequency-domain lineshapes.

Sequence 11.2 will not normally generate any echo modulation as a result of heteronuclear couplings; this is the basis of the use of homonuclear J-resolved spectroscopy to distinguish between homonuclear and heteronuclear multiplet structure. (However, echo modulation due to heteronuclear couplings can arise if there is coupling to a group of heteronuclei which are strongly coupled among themselves[7]). For simplicity, it is assumed here that the nucleus being observed is $^{13}$C and that the coupled nuclei are protons. Although the great majority of experimental applications of heteronuclear J-resolved spectroscopy are to this pair of nuclei, there are of course many other possibilities.

Two methods are commonly used to ensure that heteronuclear couplings generate echo modulation. In the "gated decoupler" method,[2,3,8,9] broadband decoupling is applied during one half only of the evolution period $t_1$; decoupling is also normally used during the preparation period (to provide the NOE) and during measurement of the free induction decay (to remove multiplet structure from $F_2$):

$$\begin{array}{ll} ^1\text{H} \leftarrow \text{Decouple} & \rightarrow \qquad\qquad \leftarrow \text{Decouple} \rightarrow \\ ^{13}\text{C} \; 90^\circ - t_1/2 - 180^\circ - t_1/2 - \text{Acquire} & \end{array} \qquad (11.3)$$

This gives a 2D spectrum in which the multiplet structure is scaled down to half of its normal width in $F_1$, but otherwise faithfully reflects the conventional spectrum, even where there is strong proton–proton coupling.

The second, "proton flip", technique[3,8,10] uses a 180° pulse to invert the coupled heteronuclei at the midpoint of the evolution period; again, decoupling is normally used during the preparation and detection periods:

$$\begin{array}{ll} ^1\text{H} \leftarrow \text{Decouple} \rightarrow \; 180^\circ & \qquad\qquad \leftarrow \text{Decouple} \rightarrow \\ ^{13}\text{C} \quad 90^\circ - t_1/2 - 180^\circ - t_1/2 - \text{Acquire} & \end{array} \qquad (11.4)$$

Here, the multiplet structure appears without any scaling, but only matches that in the 1D spectrum if the heteronuclei (here protons) are weakly coupled among themselves. The analysis of strongly coupled proton flip J-resolved spectra is discussed in 11.3.2, and closely parallels the analysis for the homonuclear case.

## 11.2 HISTORICAL REVIEW

The earliest use of Fourier transformation of the dependence of echo amplitude on the spin echo delay $t_1$ was the "J spectroscopy" experiment of Freeman and Hill.[11] This involved measuring the amplitude of the signal at the peak of the echo for a series of equally spaced values of $t_1$, and Fourier transforming with respect to $t_1$ to generate a "J-spectrum" in which chemical shifts and line broadening due to field inhomogeneity were suppressed. This experiment is of little practical utility because all the multiplets in a spectrum are superimposed, so that only the simplest spin systems can be studied. The effect of measuring just the single data point at the maximum of the echo is equivalent to carrying out an integral projection of a 2D J-resolved spectrum onto the $F_1$ axis.

The first two-dimensional experiments to use spin echoes were reported in Aue, Bartholdi, and Ernst's classic introductory paper[12] on 2D NMR; these were effectively COSY experiments with 180° mixing pulses. Proper homonuclear J-resolved spectroscopy was introduced a few months later,[1] in a communication which pointed out the possibility of obtaining a "decoupled" proton spectrum from a 45° projection. The first heteronuclear experiments were proposed independently by Freeman and coworkers shortly afterward.[2] Heteronuclear J-resolved spectroscopy proved to be a useful vehicle for the technical development of 2D NMR,[13] because it required only modest data storage.

The observation of artifacts caused by imperfect 180° pulses prompted the development of EXORCYCLE,[14] one of the first and most widely used phase cycling techniques; the acronym derived from the use of the terms "ghost" and "phantom" for the spurious signals. The differences in multiplet structure between gated decoupler and proton flip heteronuclear J-resolved spectra seen in the presence of strong proton–proton coupling[8–10] led to the development of analytical solutions and numerical software for calculating strongly coupled homonuclear, and proton flip heteronuclear, J-resolved spectra.[10,15,16] Heteronuclear J-resolved spectroscopy was also the vehicle for the early investigations of the problem of lineshapes in phase-sensitive 2D spectra. Phase modulation leads to "phasetwist" lineshapes, which are the inseparable mixture of 2D absorption and dispersion mode lineshapes.[13] This problem can be cured in heteronuclear J-resolved spectra (and, at a very significant cost in sensitivity, in homonuclear spectra; see 11.5.2) by combining results from two experiments which have opposite senses of precession in $t_1$; the apparent sense of precession can be reversed either by adding a second 180° pulse at the end of the evolution period,[17] or, in the gated decoupler experiment, by changing from decoupling during one half of $t_1$ to decoupling in the other.[18] Such expedients are actually seldom used in heteronuclear J-resolved spectroscopy, because in $F_2$-decoupled experiments, phase-sensitive $F_1$ cross-sections (which can be phased to absorption mode because they pass through the midpoints of the phasetwisted lineshapes) can usually be obtained free of overlap from neighboring signals in $F_2$. The recently developed homonuclear analog, using slice-selective 180° pulses (see 11.5.2), may however prove more popular.

With the introduction of more powerful spectrometer computers, J-resolved spectroscopy was quickly eclipsed by the more powerful and general class of correlated 2D experiments such as COSY and NOESY, but nevertheless a number of useful extensions have been demonstrated. Making the 180° proton pulse of sequence 11.4 selective restricts the modulation of the spin echo to couplings to protons with a particular chemical shift.[19] If the carbon and proton 180° pulses of a proton flip experiment are replaced by a BIRD sequence,[20] the refocusing can be made selective for either long-range or one-bond heteronuclear couplings. This is known as *semiselective J spectroscopy*,[21] giving J-resolved spectra in which, depending on the relative phases of the pulses in the BIRD sequence, either the one-bond or the longer range couplings are removed from the $F_1$ dimension, thereby simplifying analysis. Again, strong proton–proton coupling can complicate spectra very considerably, but numerical simulations can be performed;[22] the large number of lines produced can actually be an advantage because it increases the accuracy with which spin system parameters may be derived.

Another extension is known as *indirect J-spectroscopy*;[23,24] this adds a polarization transfer step to a proton spin echo, transferring the proton J-modulation to carbon-13 signals. This works well where the carbon-13 satellites in the proton spectrum are weakly coupled, allowing the clean resolution of individual proton multiplets even in systems where the proton spectrum is completely unresolved. However, it has been little used, and for most purposes, a high $F_2$ resolution HMQC experiment[25] is preferable; this does not give any proton linewidth improvement but is quicker, and doubles the chances of avoiding strong coupling if run without carbon-13 decoupling in $t_2$.

## 11.3 THEORY

### 11.3.1 Weak Coupling

Consider first a weakly coupled homonuclear system of two spins-1/2 I and S; the energy level diagram and spectrum are shown in Figure 11.1. There are two I transitions, one for the half of the spin systems in which S is in the $\alpha$ state and one for those in which it is $\beta$, and a similar pair of S transitions. Initially, the magnetizations for the four transitions will be at equilibrium; the state of the spin system may be represented in the product operator formalism[26] as

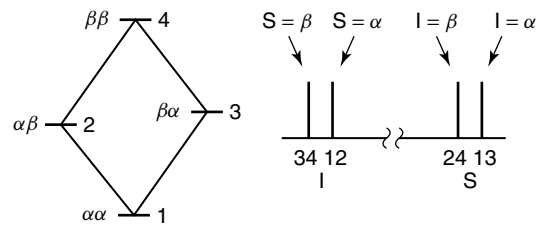


**Figure 11.1.** Energy level diagram and spectrum for a weakly coupled IS system of two spins −1/2.

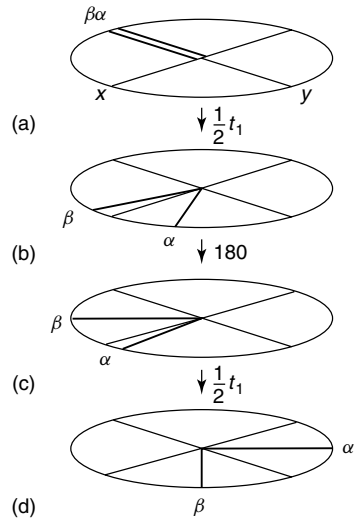


**Figure 11.2.** Motions of the two I magnetizations in a weakly coupled IS system of two spins −1/2 during sequence (11.2).

$I_z + S_z$, and the four magnetizations will point along the $z$ direction in the rotating frame of reference. The initial 90° pulse of sequence 11.2 will rotate the four magnetizations down to the $-y$-axis of the rotating frame to give $-I_y - S_y$; the I spin magnetizations are shown diagrammatically in Figure 11.2(a). During the first half of the evolution period the chemical shifts of spins I and S will cause the magnetizations to precess through angles $\phi_I = \pi\delta_I t_1$ and $\phi_S = \pi\delta_S t_1$ radians respectively, where $\delta_I$ and $\delta_S$ are the offsets from resonance in hertz of the two spins. The scalar coupling $J_{IS}$ will cause the two components of each multiplet to diverge by an angle $\theta_1 = \pi J_{IS} t_1$ radians, giving the state

$$\begin{aligned} &- I_y \cos\phi_I \cos(\theta_1/2) + I_x \sin\phi_I \cos(\theta_1/2) \\ &+ 2I_x S_z \cos\phi_I \sin(\theta_1/2) + 2I_y S_z \sin\phi_I \sin(\theta_1/2) \\ &- S_y \cos\phi_S \cos(\theta_1/2) + S_x \sin\phi_S \cos(\theta_1/2) \\ &+ 2S_x I_z \cos\phi_S \sin(\theta_1/2) + 2S_y I_z \sin\phi_S \sin(\theta_1/2) \end{aligned} \quad (11.5)$$

for which the I magnetizations are shown in Figure 11.2(b); for the time being, relaxation will be neglected. The 180° pulse, applied about the $x$-axis in the rotating frame, will have two effects. It will change the signs of all the terms in $I_y$ and $S_y$, reflecting the corresponding magnetization vectors about the $xz$ plane of the rotating frame. It will also invert all terms in $I_z$ and $S_z$; this corresponds to interchanging $\alpha$ and $\beta$ spins, so that for example the I magnetization that is associated with transition 12 before the 180° pulse (for which S is in the $\alpha$ state) is transferred to transition 34 ($S = \beta$), giving the situation shown in Figure 11.2(c).

During the second half of the evolution period the I and S magnetizations will again precess through angles $\phi_I$ and $\phi_S$ respectively, and the two components of the I and S pairs will again diverge by $\theta_1$ radians. The effect of the chemical shift precession during the second half of $t_1$ exactly matches the shift precession during the first half, so that in the absence of any coupling $J_{IS}$ all four magnetization would refocus along the $-I_y$ axis. In the presence of a coupling, the two components of the I and S multiplets end up disposed symmetrically either side of the $-I_y$ axis, $2\theta_1$ radians apart (Figure 11.2d), giving the state $+I_y \cos\theta_1 - 2I_x S_z \sin\theta_1 + S_y \cos\theta_1 - 2S_x I_z \sin\theta_1$. The signal at time $t_1$ is thus unaffected by chemical shifts (or inhomogeneity of the static magnetic field): a spin echo is produced which is modulated only by the scalar coupling $J_{IS}$. Each multiplet is a mixture of in-phase absorption mode signals ($I_y$) and antiphase dispersion signals ($2I_x S_z$); the net effect of the modulated spin echo is to multiply one multiplet component by a phase factor $e^{i\pi J_{IS} t_1}$ and the other by $e^{+i\pi J_{IS} t_1}$.

At time $t_1$, the second half of the modulated spin echo is recorded as a free induction decay $S(t_2)$. Neglecting relaxation, the complex signal $S(t_1, t_2) = M_y - iM_x$ recorded can then be written

$$\begin{aligned} S(t_1, t_2) = 1/2 \big[ &e^{i\pi J_{IS} t_1} e^{i(2\pi\delta_I + \pi J_{IS})t_2} \\ &+ e^{-i\pi J_{IS} t_1} e^{i(2\pi\delta_I - \pi J_{IS})t_2} \\ &+ e^{i\pi J_{IS} t_1} e^{i(2\pi\delta_S + \pi J_{IS})t_2} \\ &+ e^{-i\pi J_{IS} t_1} e^{i(2\pi\delta_S - \pi J_{IS})t_2} \big] \end{aligned} \quad (11.6)$$

which consists of four signals with frequency coordinates $(F_1, F_2)$ of $(J_{IS}/2,\ \delta_I + J_{IS}/2)$, $(-J_{IS}/2,\ \delta_I - J_{IS}/2)$, $(J_{IS}/2,\ \delta_S + J_{IS}/2)$ and $(-J_{IS}/2,\ \delta_S - J_{IS}/2)$: the signals are dispersed according to their normal frequencies $\delta \pm J_{IS}/2$ in $F_2$, and with just their multiplet structure $\pm J_{IS}/2$ in $F_1$. The extension to larger spin systems is straightforward.

The same logic can be applied to heteronuclear J-resolved experiments. The analysis of the proton flip method parallels that for the homonuclear case, except that the initial 90° pulse affects only (say) spin I, so that all terms in $S_x$ and $S_y$ disappear. In the gated decoupler method, the use of broadband S spin decoupling during the first half of the evolution

period suppresses the effects of $J_{IS}$ in the first half of $t_1$, so that the frequencies in $F_1$ are halved to $\pm J_{IS}/4$. In both methods, broadband decoupling is normally used during $t_2$ to remove multiplet structure from $F_2$.

### 11.3.2 Strong Coupling

In the presence of strong coupling the simple analysis in the preceding section breaks down, and it is generally necessary to use density matrix theory. Although analytical results have been presented for some simple spin systems,[16] it is usual to employ numerical methods; a modified version of the 1D spin simulation program LAOCN3,[27] SONOFLAOCOON,[10] may be used both for simulation and for iterative analysis of strongly coupled J-resolved spectra.

Consider a system containing two weakly coupled groups of spins I and S, either of which may be strongly coupled, where only the spins I are to be observed. In the heteronuclear case (sequence 11.4) group I will generally contain a single $^{13}C$ spin, and group S the coupled protons; in the homonuclear case (sequence 11.2) all the spins will belong to group I. If the matrix representation of the component of spin angular momentum about the axis $q$ for group I is denoted $\boldsymbol{I^q}$, the initial reduced density matrix $\boldsymbol{\rho_0^I}$ for group I will be equal to some constant $m_0$ times $\boldsymbol{I^z}$ and the effect of the 90° I pulse will be to rotate $\boldsymbol{\rho_0}$ into $-m_0\boldsymbol{I^y}$. If calculations are performed in the eigenbasis, the $ij$th element of $\boldsymbol{\rho^I}$ at time $t_1/2$ will be $-m_0\exp\{i\,\pi t_1(\nu_i - \nu_j)\}\boldsymbol{I}^y_{ij}$, where $\nu_i$ is the $i$th energy eigenvalue of the spin system in hertz. If the matrix representation for 180° rotation of spins I and S is $\boldsymbol{T^{IS}}$, then the effect of the 180° I and S pulses will be to transfer coherences $\rho_{ij}$ into other coherences $\rho_{kl}$:

$$\rho_{kl} = \sum_i \sum_j \rho_{ij} \mathrm{T}^{IS*}_{ik} \mathrm{T}^{IS}_{jl} \qquad (11.7)$$

Thus at the end of the evolution period the total $y$ signal will be

$$S = -m_0 \sum_i \sum_j \sum_k \sum_l \mathrm{I}^y_{ij} \mathrm{T}^{IS}_{ik} \mathrm{T}^{IS*}_{jl} \mathrm{I}^y_{lk} \times \exp\left\{\mathrm{i}\pi t_1(\nu_i - \nu_j + \nu_l - \nu_k)\right\} \qquad (11.8)$$

The 2D J-resolved spectrum therefore consists of a series of responses $S_{ijkl}$ of $F_1$ frequencies $1/2(\nu_i - \nu_j + \nu_l - \nu_k)$, with intensities given by the preexponential terms in equation (11.8). Only when all spins are weakly coupled are the $F_1$ frequencies determined solely by coupling constants; where there is strong coupling, additional signals appear with frequencies that depend on the chemical shifts. This may lead to signals being folded in $F_1$, and they may have negative intensity. While generally referred to as *strong coupling artifacts*, these signals are not artifacts in the sense of originating from any experimental imperfection, but rather are an intrinsic feature of strongly coupled spin systems.

The calculation of a 2D J-resolved spectrum thus reduces to the diagonalization of the nuclear spin Hamiltonian, as in conventional spin simulation programmes such as LAOCN3,[27] followed by construction of the eigenbasis matrix representations of the $y$ component of angular momentum and of the 180° rotation operator. By suitable choice of the groups of spins I and S, the same program may be used to calculate both homonuclear and proton flip heteronuclear J-resolved spectra. More complex experiments such as semiselective J-spectroscopy[21,22] can be simulated by replacing $\boldsymbol{T^{IS}}$ with the matrix representation of a BIRD operator.[20]

## 11.4 APPLICATIONS

### 11.4.1 Practical Implementation

J-resolved spectroscopy is one of the easiest 2D methods to implement. Sequences 11.2 and 11.3 require only the usual calibration of the 90° observe pulse width, which is not critical; if $\alpha$ is the actual flip angle of a nominal 90° pulse, the signal obtained is proportional to $\sin\alpha\ \cos 2\alpha$. Calibration of the proton 180° pulse in sequence 11.3 can be carried out by setting $t_1$ to $1/^1J_{CH}$ and varying the proton pulse width; the signal is nulled when the flip angle is 90°, and inverted when it is 180°. For all three basic sequences the phases of the 90° pulse, 180° refocusing pulse and receiver should follow a scheme such as

**Table 11.1.** Phase cycling for sequences (11.2–11.4); phase shifts are indicated as multiples of 90° for the 90° pulse ($\phi_1$), 180° pulse ($\phi_2$) and receiver ($\phi_R$); the phase of the proton 180° pulse in sequence (4) is immaterial

| | |
|---|---|
| $\phi_1$ | 0321 1032 2103 3210 |
| $\phi_2$ | 0000 1111 2222 3333 |
| $\phi_R$ | 0123 1230 2301 3012 |

that in Table 11.1, which combines EXORCYCLE[14] and CYCLOPS.[28]

The two principal advantages of J-resolved spectroscopy are the decrease in $F_1$ linewidth afforded by suppressing $B_0$ inhomogeneity effects, and the improved ability to distinguish signals that stems from separating multiplet structure from chemical shifts. The former advantage is generally restricted to small molecules with high values of $T_2$, and is most commonly exploited in proton–carbon-13 heteronuclear J-resolved spectroscopy, while the latter is most useful in proton homonuclear J-resolved spectroscopy.

### 11.4.2 Homonuclear J-Resolved 2D Spectroscopy

Figure 11.3 shows the sugar ring region of 300 MHz proton spectra of a solution of sucrose octaacetate in deuteriochloroform. At the right is the normal 1D spectrum, together with a contour plot of the J-resolved spectrum. Pseudoecho weighting was used, with absolute value display; good results are also achievable with sine-bell weighting. Strong coupling signals are visible, for example in the region around 5.4 ppm, in addition to the expected multiplets. The effects of "tilting" the data matrix at 45° in frequency space are illustrated in the left hand contour plot of Figure 11.3, which shows the J-resolved spectrum after applying equation (11.1). At the far left of Figure 11.3 the results of integrating, or "projecting", the tilted spectrum along the $F_1$ direction to give a "proton-decoupled proton" spectrum are shown; again, strong coupling "artifacts" are visible, for example around 5.4 ppm.

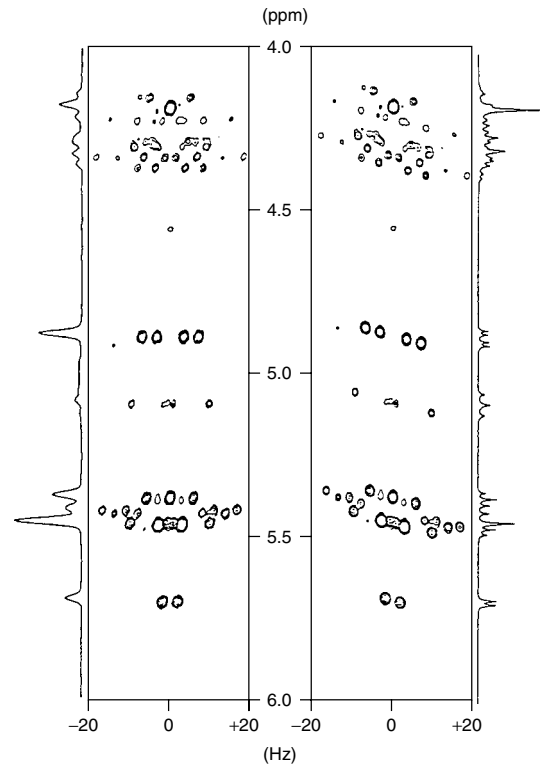


**Figure 11.3.** 300 MHz proton spectra of sucrose octaacetate. From right to left: normal 1D spectrum; J-resolved spectrum; tilted J-resolved spectrum; and $F_2$ projection of the tilted J-resolved spectrum. (Note that most NMR software reverses the signs of frequencies in $F_1$, because of the prevalence of *N*-type coherence transfer pathways in 2D correlation experiments; here the signs have been corrected).

### 11.4.3 Heteronuclear J-Resolved 2D Spectroscopy

The two classical uses of heteronuclear J-resolved spectroscopy are with low $F_1$ resolution for the determination of multiplicity, and with high $F_1$ resolution for the measurement of long-range proton-$^{13}$C couplings in small molecules. DEPT is now generally preferred for multiplicity determination, but J-resolved spectroscopy remains the method of choice for high-resolution measurements of $^nJ_{CH}$. One advantage of heteronuclear J-resolved spectroscopy for multiplicity determination is that it gives clear results in the presence of $^{13}$C shift degeneracy: Figure 11.4 shows the contour plot of the gated decoupler spectrum of the solution of cholesteryl acetate in deuteriochloroform, together with an expanded stacked trace plot of an overlapping region showing the coincidence of a methine and a methylene signal at about 29 ppm.

### 11.4.4 Semiselective J-Resolved 2D Spectroscopy

Figure 11.5 shows experimental and calculated cross sections through a high-resolution heteronuclear semiselective 2D J-resolved spectrum of thiophene in acetone-$d_6$. One-bond couplings have been suppressed by choosing phases 0, 0, and 180° for

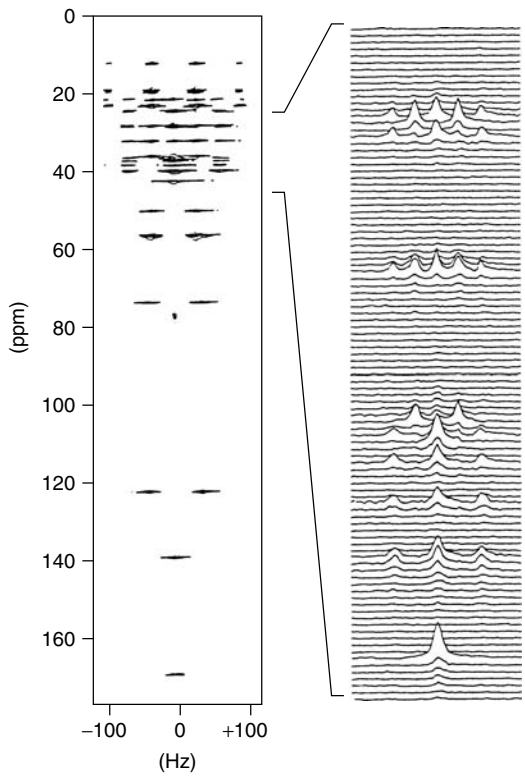


**Figure 11.4.** Gated decoupler heteronuclear J-resolved 75 MHz $^{13}$C spectrum of cholesteryl acetate, showing a stacked trace plot of an expanded region.

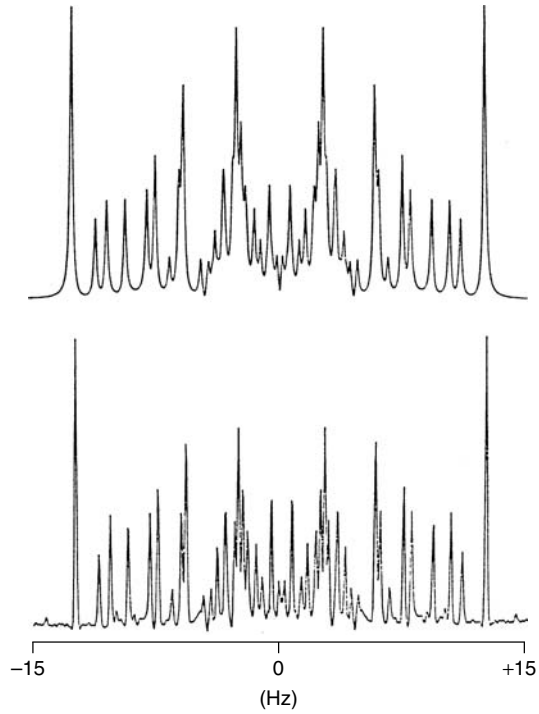


**Figure 11.5.** Semiselective one-bond suppressed heteronuclear J-resolved $^{13}$C spectra for C-2 of thiophene (60% v/v solution in deuterioacetone), (top) calculated and (bottom) experimental. The sequence of ref. 21 was used on a 400 MHz spectrometer.

the three successive proton pulses of the BIRD sequence.[20] The cross sections illustrate both the high resolution achievable, and the complexity of the spectra that can result even from relatively small strongly coupled spin systems. The theoretical trace was calculated using the approach outlined in 11.3.2 the delays during the BIRD sequence allow some of the strong coupling responses to appear in dispersion mode.

## 11.5 RECENT ADVANCES

### 11.5.1 Suppression of Strong Coupling "Artifacts"

As explained in 11.3.2, where there is strong coupling, 2D J-resolved spectra show responses whose $F_1$ frequencies depend on chemical shifts as well as coupling constants. In spin systems with very strong coupling, the concept of a J-resolved spectrum breaks down: chemical shift differences are comparable to scalar couplings, individual multiplets for different spins cannot be distinguished, and the resulting spectra can be highly complex. Although it may be still useful to record a J-resolved spectrum, for example to allow very accurate measurement of coupling constants by iterative fitting, it is not possible to separate multiplet structure from chemical shifts in such systems. However, for less strongly coupled spin systems, where second-order effects distort the amplitudes of the multiplet components in the conventional spectrum without greatly perturbing their frequencies, the effect on J-resolved spectra is to introduce extra signals in the $F_1$ domain.

In the simple case where two spins A and B are moderately strongly coupled, extra responses will appear in the J-resolved spectrum at $F_1$ frequencies such that a 45° projection shows signals intermediate

in chemical shift between A and B (i.e., at positive $F_1$ for A signals and negative for B if the chemical shift of A is greater than that of B, $\delta_A > \delta_B$). A simple rationalization of these extra responses is that the eigenstates of such a spin system are no longer pure product basis states, but mixtures. While there are still only four signals in the normal spectrum, each of these partakes of some of the character of both spins A and B, because each represents coherence between eigenstates that are mixtures of product basis states. As illustrated in Figure 11.2, the twin effects of a hard 180° pulse on a weakly coupled spin A are to rotate the A magnetization vectors by 180°, and to interchange their frequencies. In an AB spin system, there is a third effect: to transfer some magnetization between A and B, giving rise to extra signals with $F_1$ frequencies shifted up (for A) or down (for B) by $\Delta/2 = \sqrt{(\delta_A - \delta_B)^2 + J^2}/2$. A clear analysis of this effect is given in Ref. 29.

The net result is that for mild strong coupling, the J-resolved spectrum of an AB spin system contains the multiplet structure that would be expected for the weak coupling AX case (with all peaks of equal amplitude), plus extra peaks displaced by $\pm\Delta/2$ in $F_1$ and with amplitudes equal to the difference between the strongly and the weakly coupled peak amplitudes in the normal spectrum. In other words, for a two-spin system, the signal amplitude difference between weak and strong coupling ends up going into the "artifact" peaks. The effect on a 45° tilted 2D spectrum is that both the component peaks of the normal multiplets and the extra signals are symmetrically distributed about $F_1 = 0$, with the latter centered in $F_2'$ on the average of the A and B chemical shifts. This symmetry may be seen in the region of Figure 11.3 around 5.4 ppm in $F_2$, where the A and B resonances of an ABMX spin system are located.

The characteristic appearance of the extra signals found in strongly coupled J-resolved spectra means that they are easily recognized, and rarely complicate the interpretation of J-resolved spectra themselves. However, such spectra are frequently used as a vehicle for obtaining the 45° projection, in which all homonuclear multiplet structure is suppressed in the weak coupling case (see also 11.5.3). Here the extra responses in the case of strong coupling complicate matters considerably, because the "artifact" peaks project to form spurious peaks at intermediate chemical shifts that could easily be misinterpreted. Keeler and coworkers have therefore developed[29] a number of ways of suppressing the extra peaks, all variants on the double spin echo experiment in which two 180° pulses are used. With mild strong coupling, each 180° pulse transfers only a small proportion of the transverse magnetization between spins. Thus in a double spin echo, the "artifact" responses are dominated by magnetization that was only transferred in one of the two echoes, and hence is displaced in $F_1$ by $\pm\Delta/4$; only a small proportion of the signal actually builds up the full displacement $\Delta/2$. Reference 29 describes several more sophisticated experiments that seek to average out the unwanted signals, but the simplest just uses two equal spin echo periods:

$$90^\circ - t_1/4 - 180^\circ - t_1/2 - 180^\circ - t_1/4 - \text{Acquire} \qquad (11.9)$$

A suitable phase cycle is the double EXORCYCLE of Table 11.2; for clean results, either a minimum of 16 transients should be used, or field gradient pulses in the ratio $-1:1:2$ inserted in the three evolution delays. Because the main strong coupling responses are now only displaced half as far in $F_1$, they no longer appear symmetrically disposed either side of $F_1 = 0$ after 45° rotation of a J-resolved spectrum, and hence they can be suppressed by symmetrization – replacing each point $S(F_1, F_2')$ by the lower of $S(F_1, F_2')$ and $S(-F_1, F_2')$. (Nonlinear data manipulations are in general best avoided, but 45° projection here relies in any case on the nonlinear operation of taking the absolute value spectrum $|S(F_1, F_2')|$.)

While the extra peaks seen in 45° projections of the J-resolved spectra of strongly coupled systems are usually easily identified and discounted in the spectra of single species, because they are weaker than the parent signals, in the spectra of mixtures

**Table 11.2.** Phase cycling for sequence (11.9) and the sequences of Figures 11.7 and 11.9; phase shifts are indicated as multiples of 90° for the 90° pulse ($\phi_1$), penultimate 180° pulse ($\phi_2$), final 180° pulse ($\phi_3$), and receiver ($\phi_R$). In the sequences of Figures 11.7(c and d), the first (BIP) 180° pulse has the phase $\phi_1$. Subscripts indicate repetition; thus $(0202\ 1313)_8$ indicates a 64-step cycle in which the sequence $(0202\ 1313)_8$ is repeated 8 times

| | |
|---|---|
| $\phi_1$ | $(0202\ 1313)_8$ |
| $\phi_2$ | $0_{16}\ 1_{16}\ 2_{16}\ 3_{16}$ |
| $\phi_3$ | $(00110011\ 22332233)_4$ |
| $\phi_R$ | $(02201331\ 02201331\ 20023113\ 20023113)_2$ |

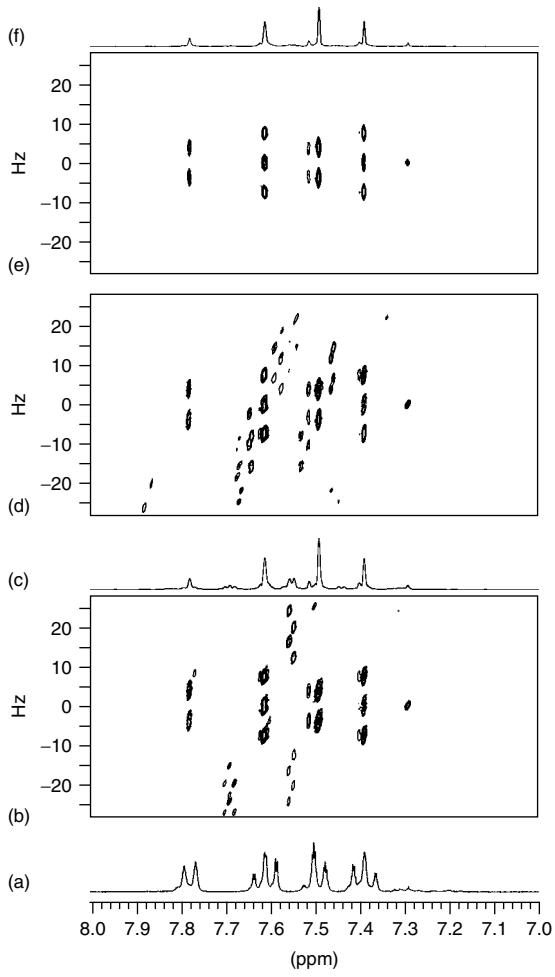


**Figure 11.6.** (a) Aromatic region of the 300 MHz proton spectrum of an impure sample of 2-ethyl-1-indanone in deuteriochloroform; (b) 45° rotated J-resolved spectrum, measured with the conventional sequence (2); (c) integral projection onto the chemical shift axis of the rotated spectrum (b); (d) 45° rotated J-resolved spectrum measured with the double spin echo sequence (9); (e) spectrum (d) after symmetrization about the axis $F_1 = 0$ and (f) integral projection onto the chemical shift axis of the rotated and symmetrized spectrum (e).

they can be much more troublesome. Figure 11.6 illustrates this for the case of 300 MHz proton NMR of an impure sample of 2-ethyl-1-indanone in deuteriochloroform. It is clear from the multiplet intensity patterns in the normal proton spectrum (a) that there is strong coupling, but not clear which of the smaller signals arise from strong coupling and which, if any, from impurities. The projection (c) of the 45°-rotated normal J-resolved spectrum (b), measured with sequence 11.2, shows a number of weak signals, but again it is far from clear which if any come from impurities. In the 45°-rotated double spin echo J-resolved spectrum (d) measured with sequence 11.9 the number of strong coupling peaks is, as expected, greater than that in spectrum (b), but on symmetrization (e), almost all of these are suppressed. It is now clear from the projection (f) that the weak signals just to the left of each of the main peaks arise from impurities and not from strong coupling. The coupling in this spin system is sufficiently strong that weak strong coupling responses, from coherences which were transferred between spins by both 180° pulses of the double spin echo, can be still just be seen in the projection (f) at around 7.55 and 7.70 ppm.

### 11.5.2 Absorption-Mode J-Resolved Spectroscopy

One of the key limitations of J spectroscopy is the need for absolute value display, which arises because the signals are phase modulated as a function of both $t_1$ and $t_2$. As explained in 11.1, this necessitates the use of severe weighting functions such as the sine bell or pseudoecho to force the envelopes of the time-domain signals into approximate symmetry. This exacts a high price in both sensitivity and resolution, and severely compromises the quantitative character of the resultant spectra. All these problems can be avoided in heteronuclear J-resolved spectroscopy, where 2D absorption mode lineshapes can be obtained either by manipulating the decoupler gating pattern or by using an extra 180° pulse to reverse the sense of phase modulation in $F_1$.[17,18] In homonuclear experiments, real-time broadband decoupling is not an option, and an extra hard 180° pulse would cause unwanted coherence transfer and hence retain rather than reverse the (homonuclear) J modulation. However, there is a simple and elegant way to make a subset of spins mimic the behavior of heteronuclei, which is to use a pulse that is both spatially and chemical shift selective to restrict the active spins to a different spatial region of the sample for each chemical shift. This unjustly neglected technique was first introduced by Zangger and Sterk[30] in an experiment for the measurement of phase sensitive

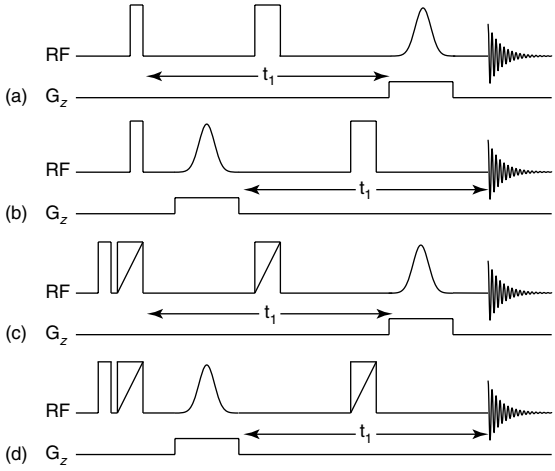


**Figure 11.7.** (a), (b) Basic conjugate pair of pulse sequences for the measurement of absorption-mode homonuclear J-resolved spectra, in which sequences (a) and (b) give equal and opposite J-modulation as a function of $t_1$; (c), (d) the corresponding conjugate pair of sequences using BIP (Broadband Inversion Pulse) refocusing pulses. Hard pulses of 90 and 180° are denoted by narrow and wide rectangular pulses respectively, soft shaped 180° pulses by a Gaussian shape, and BIP pulses by a wide rectangular pulse with a diagonal bar. For phase cycling see Table 11.2.

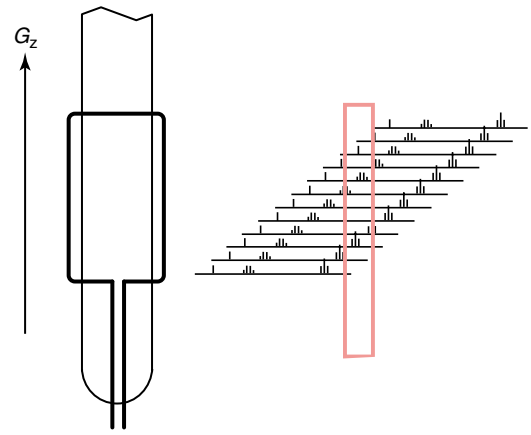


**Figure 11.8.** The use of a selective 180° pulse in the presence of a weak field gradient to excite signals with different chemical shifts at different positions in the experimental sample. The effect of the vertical field gradient $G_z$ on the active volume of the sample (indicated by schematic RF coil and sample tube at the left) is to cause the spectrum at each vertical position in the sample (right) to be centerd at a different frequency. As a result, each different chemical shift in the spectrum is on resonance with the selective 180° pulse (shaded box) only in one thin slice of the sample. The thickness of the slice excited depends on the magnitude of $G_z$ and the frequency bandwidth of the 180° pulse.

pure shift spectra (see 11.5.3), and is both a versatile pulse sequence building block and an early illustration of the potential of spatially resolved methods in high-resolution NMR (see Chapter 3). The price paid for the extra freedom this pulse sequence element gives is a significant penalty in signal-to-noise ratio, in proportion to the ratio of the width of the spectrum to the soft pulse excitation bandwidth. This last determines the smallest chemical shift difference for which decoupling is effective, and is typically of the order of 50 Hz; below this figure, strong coupling effects are likely to intrude.

Figure 11.7 illustrates the use of the 180° Zangger–Sterk pulse sequence element to allow the measurement of phase sensitive J-resolved spectra.[31] The basic sequence (Figure 11.7a and b) is a direct analog of the sequence of reference 17, in which the slice-selective 180° pulse plays the part of the extra $^{13}$C 180° pulse. Because the soft pulse applies a 180° rotation to a given chemical shift only in one thin slice of the sample (see Figure 11.8), it has no effect on the passive spins in that slice, allowing the sense of phase modulation to be reversed without any coherence transfer. Sequences (a) and (b) in Figure 11.7 form a conjugate pair in which sequence (a) gives the normal J-modulation as a function of $t_1$ and (b) the reverse; this is analogous to the use of opposite signs of field gradient pulses in many pulse sequences for phase-sensitive gradient-enhanced 2D NMR. The experimental data produced by sequences (a) and (b) can thus be combined and processed as normal for an *N*, *P*-type 2D NMR experiment. Figures 11.7(c) and (d) show a slightly more complex implementation of the same idea, in which the use of a matched pair of BIP (broadband inversion pulse) composite pulses[32] can reduce the need for phase cycling in favorable circumstances. Alternatively, and more simply, gradient pulses in the ratio $-1:1:2$ may be added to the three interpulse delays to allow the sequence to be run with no phase cycling; the only significant drawback is the introduction of a very small frequency-dependent $F_1$ phase shift, and the gradient-enhanced experiment is much more tolerant of spectrometer limitations.

Figure 11.9 illustrates the application of the pulse sequence of Figure 11.7(a) and (b), with the addition

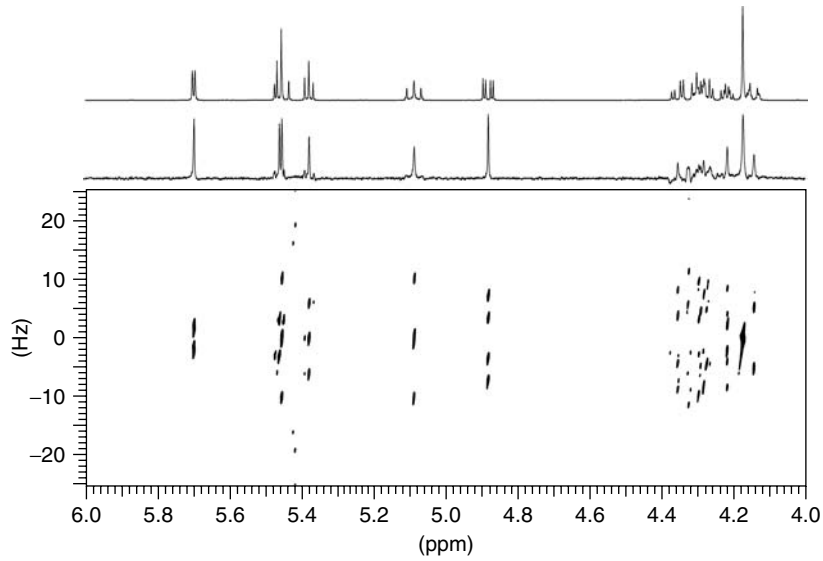


**Figure 11.9.** Ring proton region of the 500-MHz absorption-mode proton J-resolved spectrum, after 45° rotation, of a solution of sucrose octaacetate in deuteriochloroform, measured using the sequences of Figures 11.7a/b with the addition of gradient pulses with areas in the ratio $-1:1:2$ in the intervals between the three 180° pulses, with (middle) integral projection onto the chemical shift axis, and (top) conventional spectrum.

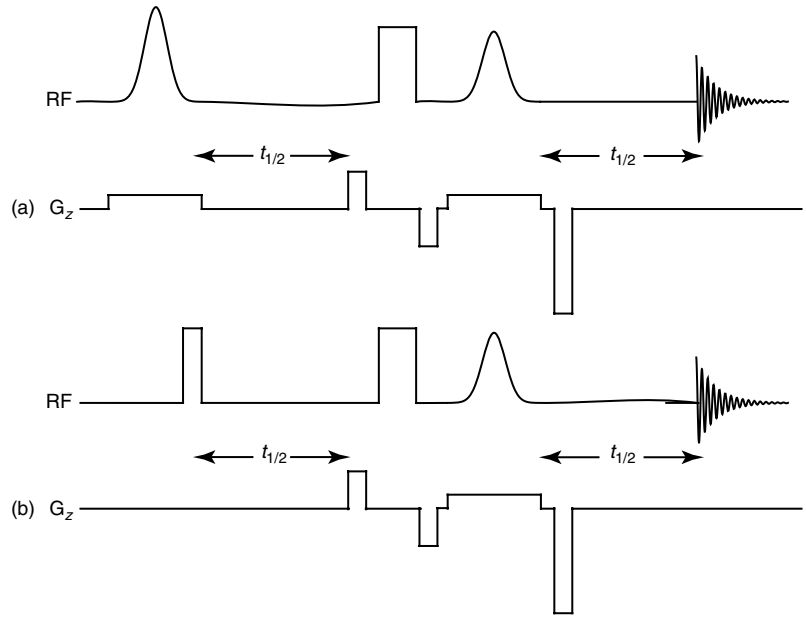


**Figure 11.10.** Pulse sequences for the measurement of pure shift spectra by the Zangger–Sterk method, with initial excitation (a) by slice-selective self-refocusing 270° Gaussian pulse, and (b) hard 90° pulse. Hard pulses of 90 and 180° are denoted by narrow and wide rectangular pulses respectively, and soft shaped 180 and 270° pulses by shorter and taller Gaussian shapes. For phase cycling see Table 11.2. For evolution times $t_1$ greater than zero, data acquisition starts at a time $\Delta t_2/2$ before the end of $t_1$.

of the field gradient pulses just described, to the ring proton region of the 500 MHz proton spectrum of sucrose octaacetate. The 45°-rotated absorption mode J-resolved spectrum (Figure 11.9c) shows quite clean 2D lineshapes, although the effects of imperfect balance between the two halves of the sequence are just visible on the strong singlet signal at 4.16 ppm. Weak strong coupling responses, analogous to those in the conventional experiment, are seen at 5.41 ppm. Comparison between the normal spectrum (Figure 11.9a) and the $F_2'$ projection (Figure 11.9b) of the 2D spectrum shows both the strengths and the limitations of the technique as a source of pure shift spectra. Clean, quantitative absorption-mode signals are obtained for weakly coupled protons. As expected, the experiment fares less well in the very crowded region around 4.35 ppm, where strong coupling causes extra signals to appear in the projection, some with negative intensity. Weak satellite signals are seen on some peaks: these have multiple causes, including strong coupling and nonideality of the soft pulse excitation spectrum. The latter problem is a feature of the Zangger–Sterk pulse sequence element, and is caused by the edges of the selected sample slice experiencing incomplete refocusing. It can be reduced by using a shaped pulse with as rectangular an excitation spectrum as possible, or eliminated by replacing the initial hard 90° excitation pulse of Figure 11.7 with a soft excitation which has a lower bandwidth than the selective 180° refocusing pulse, as in Zangger and Sterk's original experiment.[30] The principal limitation of the experiments of Figure 11.7 is that of necessity they sacrifice a great deal of signal-to-noise ratio (approximately a factor of 300 for Figure 11.9), because the signal observed is restricted to a thin slice of the sample for each point in the spectrum. The extent of this sacrifice depends on the ratio of the spectral width to the selective pulse bandwidth used, the latter being determined as noted above by the smallest chemical shift difference between coupled spins for which 2D absorption mode signals are required.

### 11.5.3 "Pure Shift" Spectra

Since its inception, homonuclear J-resolved spectroscopy has been seen partly as an aid to the analysis of complex, overlapping spectra, and partly as a route to a spectrum in which all homonuclear couplings have been suppressed. Routes to such "pure shift" spectra have been sought since the earliest days of Fourier transform NMR, and by many of the most distinguished names in the field. It is something of a paradox that when, after over 25 years of at best qualified success in this area, Zangger and Sterk finally produced a practical experiment[29] that met almost all of the desiderata for a pure shift NMR experiment (phase sensitive display, broadband decoupling of all resonances, quantitative results), the shift of attention to the burgeoning field of multidimensional NMR techniques meant that their achievement passed almost unnoticed.

As noted in 11.5.2, the Zangger–Sterk pulse sequence element uses a selective 180° pulse applied

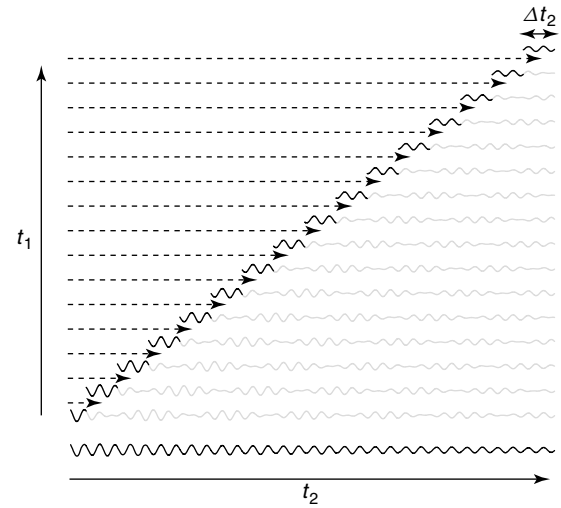


**Figure 11.11.** Construction of a composite free induction decay (bottom trace) from "chunks" of time-domain data acquired with different evolution times $t_1$ (upper traces). The composite decay is built up by first recording for a time $\Delta t_2/2$ the signal generated by using the sequence of Figure 11.10(a) or 11.10(b) with zero evolution time $t_1$. Successive segments of experimental free induction decay lasting a time $\Delta t_2/2$ are then appended to this for evolution times $t_1 = \Delta t_2$, $t_1 = 2\Delta t_2$, $t_1 = 3\Delta t_2$, etc., where $\Delta t_2 \ll 1/J$, until a complete composite decay has been built up. Only the initial $\Delta t_2/2$ or $\Delta t_2$ of each experimental free induction decay is used, as highlighted. The sequences of Figure 11.10 refocus the J evolution of the signals at time $t_1$; because J modulation is slow, it has little effect on the signal recorded during the interval $t_1 - \Delta t_2/2$ to $t_1 + \Delta t_2/2$, so the fully decoupled free induction decay can be constructed using a relatively small number of values of $t_1$. (For the purposes of illustration, the value of $\Delta t_2$ used in calculating the traces shown above was $0.4/J$, rather larger than would be used in practice).

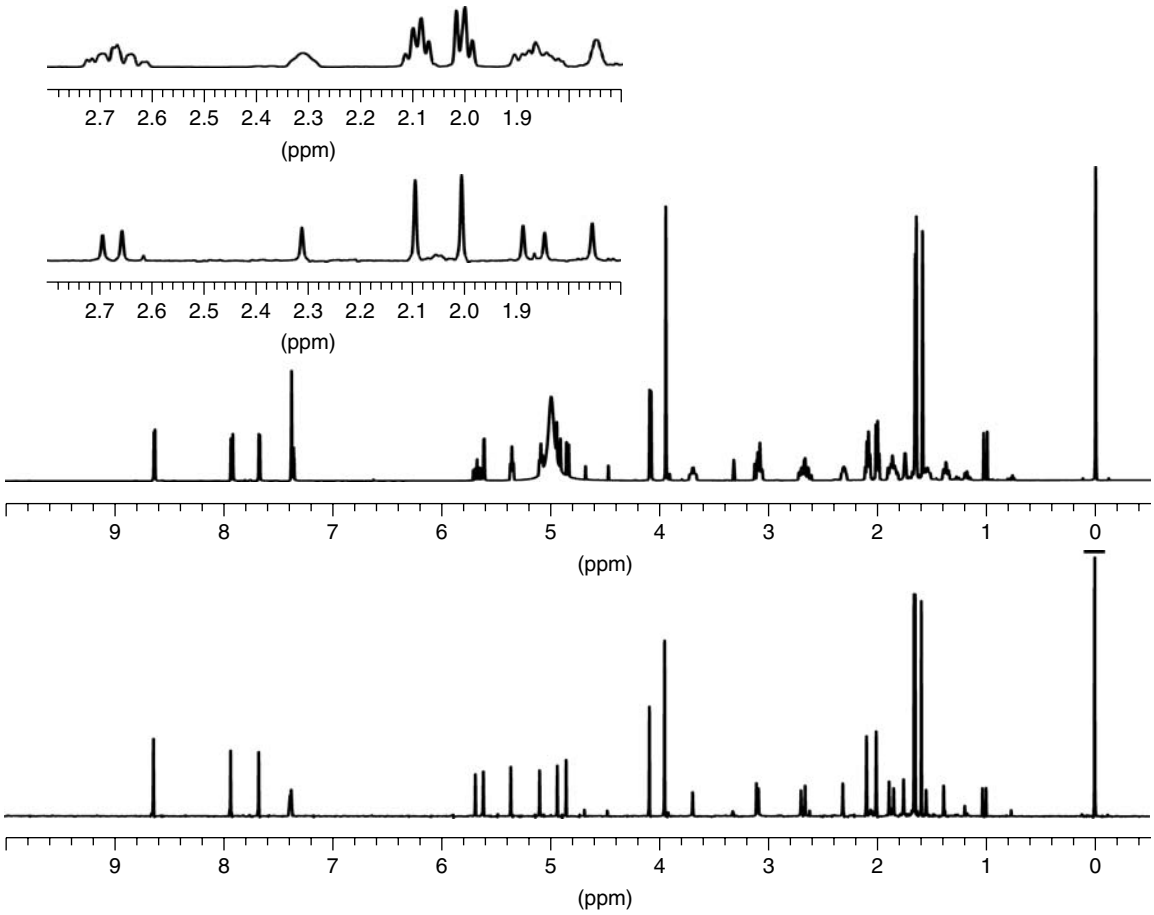


**Figure 11.12.** (Upper main trace) 500 MHz proton spectrum of a solution of quinine, geraniol, camphene and tetramethylsilane in deuteriomethanol, and (lower main trace) 500 MHz pure shift spectrum of the same sample measured using the sequence of Figure 11.10b, with (insets top left) expansions of the aliphatic region 1.7–2.8 ppm. Only small strong coupling artifacts are visible (at 1.87 and 2.05 ppm) because of the highly selective (20 Hz bandwidth)180° pulse used. Experimental data kindly provided by Dr Juan Aguilar.

in the presence of a field gradient just strong enough that each chemical shift of interest is on resonance at a different position in the sample (Figure 11.8). This spatial- and chemical shift-selective refocusing pulse is combined with a hard 180° pulse so that the net effect is to rotate all spins except those of interest through 180°. Thus when this pair of pulses is placed at the center of an evolution period $t_1$, the net effect is that signals are phase modulated by their chemical shifts but unaffected by homonuclear coupling (provided that the soft 180° pulse is sufficiently selective to affect one chemical shift only at a time). An experiment that used this pulse sequence to map out the chemical shift modulations point by point, as in a two-dimensional NMR experiment, would be extremely slow, but Zangger and Sterk noted that the J evolution is relatively slow compared to the chemical shift. This means that instead of acquiring one data point at a time, a "chunk" of free induction decay lasting a time $\Delta t_2 \ll 1/J$ containing tens of data points can be recorded, greatly reducing the number of different $t_1$ values required. Practical sequences are shown in Figure 11.10(a) with a shaped excitation pulse for the cleanest results, and 11.10(b) with a hard 90° excitation pulse where occasional artifacts can be tolerated if two spins have chemical shifts that

differ by the bandwidth of the selective 180° pulse. A composite free induction decay is then constructed from successive experiments in which $t_1$ is incremented by $\Delta t_2$, as illustrated in Figure 11.11. This composite decay can be Fourier transformed as normal to yield an approximately quantitative absorption mode pure shift spectrum, as in Figure 11.12. Field gradient pulses are used to ensure that the only signals detected are from spins that are rotated through 180° by both the hard and the soft 180° pulses, so that the net effect is that only the spins outside the sample slice containing the spins of interest are inverted.

Pure shift methods such as the Pell-Keeler phase-sensitive 2D J spectroscopy or the Zangger–Sterk sequences are of considerable potential utility in their own right, simplifying complex spectra and aiding assignment and analysis, but they are particularly useful where spectral overlap causes special problems. A particular case in point is DOSY (see Chapter 36), where even mild overlap between signals leads to incorrect estimation of diffusion coefficients. Both the Zangger–Sterk method and a pure shift method based on anti-$z$ COSY have been successfully applied to DOSY,[33,34] and it is straightforward to extend the sequences of Figure 11.7 to generate 3D absorption-mode 2D J-resolved DOSY or 45°-projected 2D pure shift DOSY spectra.

## RELATED ARTICLES IN THE ENCYCLOPEDIA OF MAGNETIC RESONANCE

**Field Gradients and Their Application**

**Spin Echo Spectroscopy of Liquid Samples**

## REFERENCES


1. W. P. Aue, J. Karhan, and R. R. Ernst, *J. Chem. Phys.*, 1976, **64**, 4226.
2. G. Bodenhausen, R. Freeman, and D. L. Turner, *J. Chem. Phys.*, 1976, **65**, 839.
3. L. Müller, A. Kumar, and R. R. Ernst, *J. Magn. Reson.*, 1977, **25**, 383.
4. H. Y. Carr and E. M. Purcell, *Phys. Rev.*, 1954, **94**, 630.
5. A. Bax, R. Freeman, and G. A. Morris, *J. Magn. Reson.*, 1981, **43**, 333.
6. J. C. Lindon and A. G. Ferrige, *Prog. Nucl. Magn. Reson. Spectrosc.*, 1980, **14**, 27.
7. A. Kumar and R. R. Ernst, *Chem. Phys. Lett.*, 1976, **37**, 162.
8. G. Bodenhausen, R. Freeman, R. Niedermeyer, and D. L. Turner, *J. Magn. Reson.*, 1976, **24**, 291.
9. R. Freeman, G. A. Morris, and D. L. Turner, *J Magn. Reson.*, 1977, **26**, 373.
10. G. Bodenhausen, R. Freeman, G. A. Morris, and D. L. Turner, *J. Magn. Reson.*, 1977, **28**, 17.
11. R. Freeman and H. D. W. Hill, *J. Chem. Phys.* **54**, 301 (1971).
12. W. P. Aue, E. Bartholdi, and R. R. Ernst, *J. Chem. Phys.*, 1976, **64**, 2229.
13. G. Bodenhausen, R. Freeman, R. Niedermayer, and D. L. Turner, *J. Magn. Reson.*, 1977, **26**, 133.
14. G. Bodenhausen, R. Freeman, and D. L. Turner, *J. Magn. Reson.*, 1977, **27**, 511.
15. (a) A. Kumar, *J. Magn. Reson.*, 1978, **30**, 227; (b) *J. Magn. Reson.*, 1980, **40**, 413.
16. G. Bodenhausen, R. Freeman, G. A. Morris, and D. L. Turner, *J. Magn. Reson.*, 1978, **31**, 75.
17. P. Bachmann, W. P. Aue, L. Müller, and R. R. Ernst, *J. Magn. Reson.*, 1977, **28**, 29.
18. R. Freeman, S. P. Kempsell, and M. H. Levitt, *J. Magn. Reson.*, 1979, **34**, 663.
19. A. Bax and R. Freeman, *J. Am. Chem. Soc.*, 1982, **104**, 1099.
20. J. R. Garbow, D. P. Weitekamp, and A. Pines, *Chem. Phys. Lett.*, 1982, **93**, 504.
21. A. Bax, *J. Magn. Reson.*, 1983, **52**, 330.
22. P. Sándor, G. A. Morris, and A. Gibbs, *J. Magn. Reson.*, 1989, **81**, 255.
23. G. A. Morris, *J. Magn. Reson.*, 1981, **44**, 277.
24. V. Rutar, *J. Magn. Reson.*, 1984, **50**, 413.
25. A. Bax and S. Subramaniam, *J. Magn. Reson.*, 1986, **67**, 565.
26. O. W. Sørensen, G. W. Eich, M. H. Levitt, G. Bodenhausen, and R. R. Ernst, *Prog. Nucl. Magn. Reson. Spectrosc.*, 1983, **16**, 163.
27. A. A. Bothner-By and S. M. Castellano, in *Computer Programs for Chemistry*, ed D. F. DeTar, Benjamin, New York, 1968, Vol. **1**.
28. D. I. Hoult and R. E. Richards, *Proc. R. Soc. Lond., Ser. A*, 1975, **344**, 311.

29. M. J. Thrippleton, R. A. E. Edden, and J. Keeler, *J. Magn. Reson.*, 2005, **174**, 97.

30. K. Zangger and H. Sterk, *J. Magn. Reson.*, 1997, **124**, 486.

31. A. J. Pell and J. Keeler, *J. Magn. Reson.*, 2007, **189**, 293.

32. M. A. Smith, H. Hu, and A. J. Shaka, *J. Magn. Reson.*, 2001, **151**, 269.

33. A. J. Pell, R. A. E. Edden, and J. Keeler, *Magn. Reson. Chem.*, 2007, **45**, 296.

34. M. Nilsson and G. A. Morris, *Chem. Commun.*, 2007, 933.